CHAPTER 4

Microstructural Characterization and Microhardness variation after USSP treatment

4.1 INTRODUCTION

This chapter discusses the effects of ultrasonic shot peening on microstructure, surface roughness, and microhardness. Solution treated (900 °C for 1 hour) and water quenched Ti-13Nb-13Zr alloy samples were exposed to ultrasonic shot peening (USSP) with hard steel balls of 3 mm diameter for a duration ranging from 15 to 360 seconds. Optical, scanning electron, and transmission electron microscopy techniques were used to investigate the changes in the microstructure. XRD analysis of the shot peened surfaces was also performed to determine whether any phase transformation had occurred as a result of the USSP.

4.2 MICROSTRUCTURAL CHARACTERIZATION

Disc shaped samples of 11 mm diameter and 5 mm thickness were cut from the heat treated blank and mechanically polished. These samples were designated as "Un-USSP". Part of the Un-USSP samples were USSP treated with steel shots of 3 mm diameter by the ultrasonic horn (Stressonic Stress Voyager, France) vibrating at a constant frequency of 20 kHz with amplitude of 80 μm. The duration of USSP was varied from 15 to 360 s. The designations of the different samples are shown in Table 4.1. The microstructure of the Un-USSP sample was examined using optical and scanning electron microscope (SEM) after etching the polished surface with Kroll's reagent. In-depth analysis of microstructure of the surface region was carried out using transmission

electron microscope (Technai G2) at 200 kV. X-ray diffraction (XRD) analysis was done prior to and also post USSP treatment, using Empyrean Panalytical X-ray diffractometer with Co Kα radiation to determine the phase constituents.

Table 4.1 Designations of the USSP treated specimens.

USSP Treatment Duration (seconds)	**Designation**
15	USSP15
30	USSP30
60	USSP60
120	USSP120
240	USSP240
360	USSP360

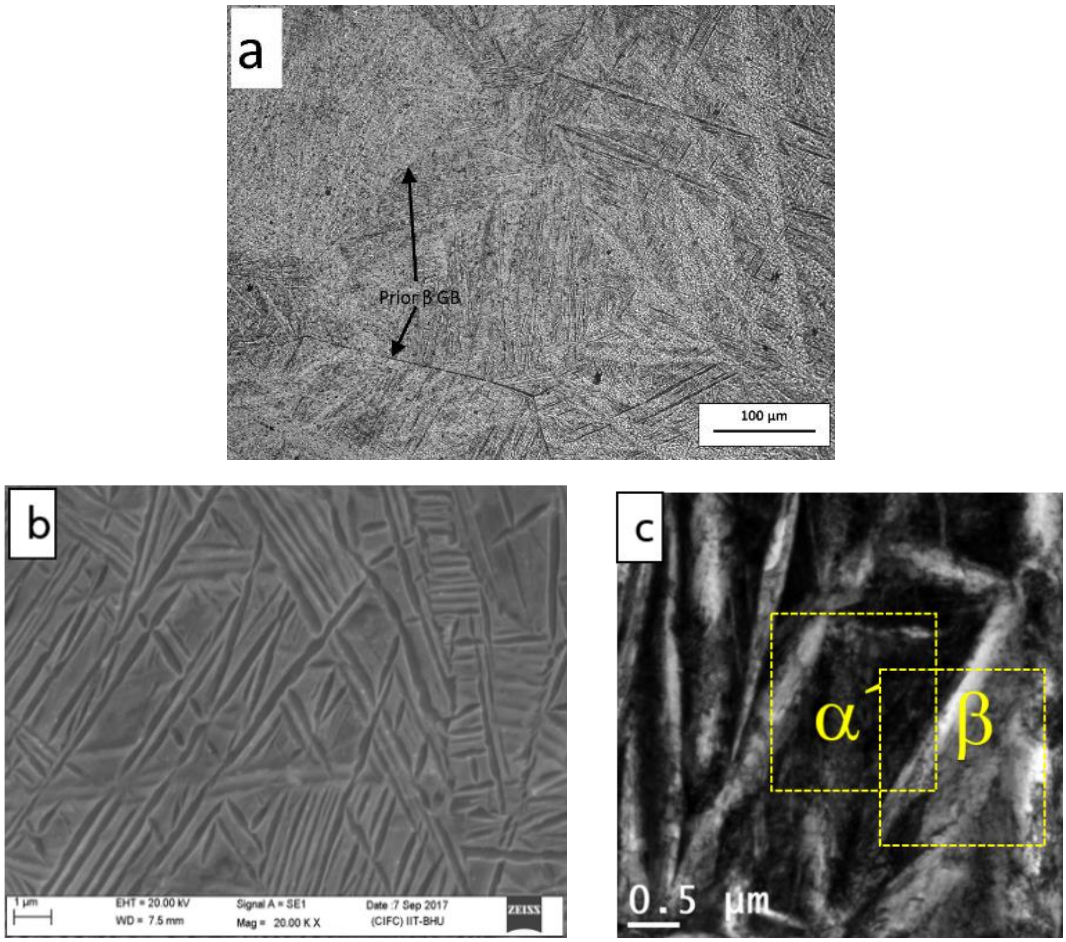

Figure 4.1 (a) Optical, (b) SEM, and (c) TEM micrographs of the Un-USSP (900WQ) sample.

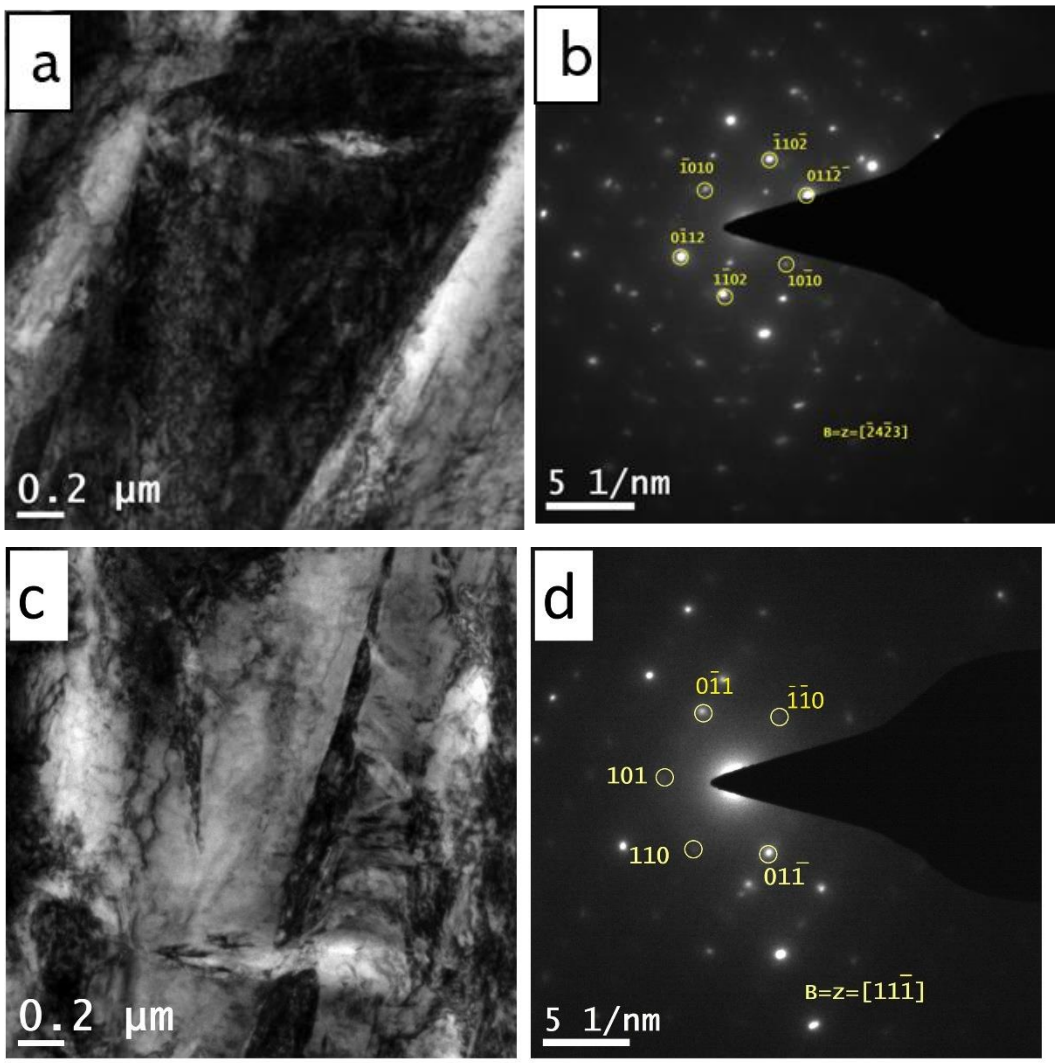

Figure 4.2 TEM micrographs of (a) of α′(hcp) and (c) β (bcc) phases, along with respective SAED patterns shown in (b) and (d).

Figure 4.1 displays (a) optical, (b) SEM and (c) TEM micrographs of the Un-USSP sample in the solution treated (900°C 1 h) and water quenched condition. It shows prior coarse β-grained microstructure with grain size (mean intercept length) of 198±04 μm. It also reveals acicular α' (hcp martensite) morphology in the large β grains. The α′ and β (bcc) phases were further confirmed through typical TEM micrographs and respective SAED patterns, shown in Figure 4.2.

The XRD peaks in Figures 4.3 and 4.4 show the respective phases of the Un-USSP and USSP treated conditions. The various XRD peaks in the USSP treated

conditions show peak broadening, resulting from grain refinement, increased micro strain, and instrumental broadening [218].

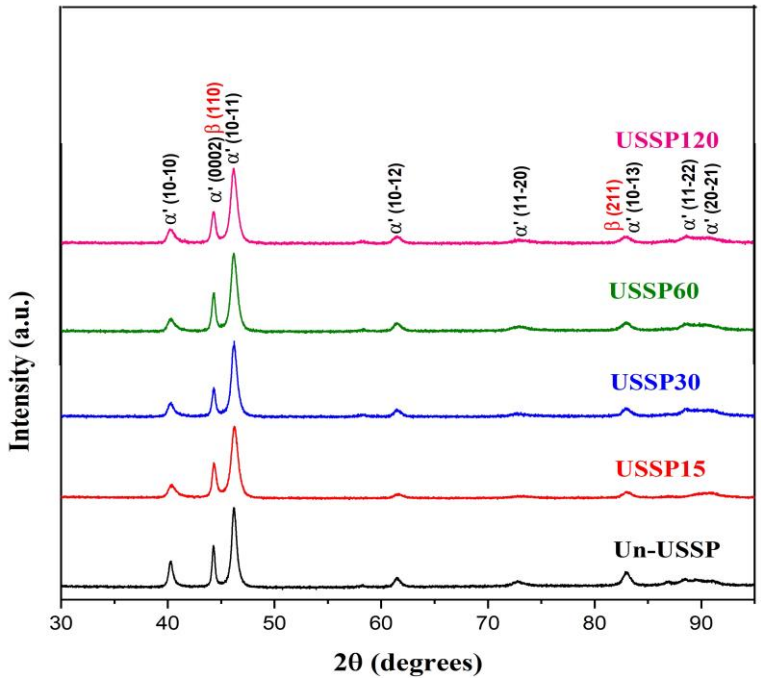

Figure 4.3 XRD profiles of the Un-USSP and USSP treated specimens (used for corrosion study).

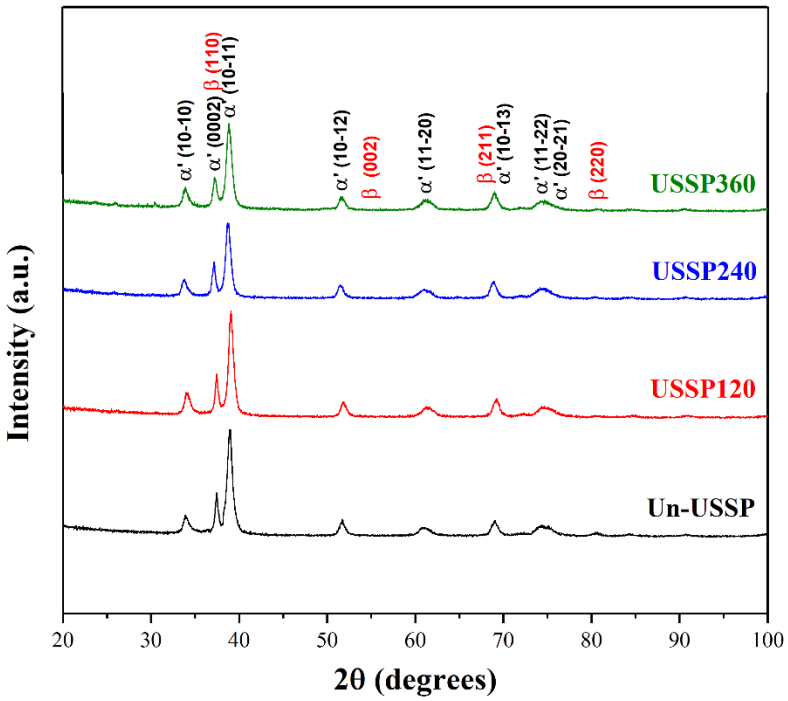

Figure 4.4 XRD profiles of the Un-USSP and USSP treated specimens (used for low cycle fatigue study).

The average crystallite size was determined using PANalytical X'Pert HighScore Plus software, after deconvolution and peak fitting of the XRD peaks with the help of Gaussian and Laurentian equation from the fitted six X-ray diffraction peaks of the hcp α′ martensite, $(10\bar{1}0), (0002), (11\bar{2}0), (10\bar{1}1), (10\bar{1}2)$ and $(11\bar{2}0)$ using Scherrer and Wilson equation [219],

$$t = \frac{0.9\lambda}{B cos\theta} \quad \text{(Equation 4.1)}$$

where t is effective size of the crystallite, λ is wavelength of the X-ray radiation, θ is Bragg's angle, and B is peak line broadening. The estimation of micro-strain from the integral breadth of XRD peaks was done using the Williamson-Hall equation [220],

$$Bcos\theta = \left[\frac{0.9\lambda}{t}\right] + [4\varepsilon . sin\theta] \quad \text{(Equation 4.2)}$$

where ε is root mean square of micro-strain. The average value of crystallite size and micro-strain was calculated and listed in Table 4.2.

Table 4.2 Calculated crystallite size and mean micro-strain of the USSP treated specimens.

Treatment Condition	Crystallite Size (nm)	Mean Microstrain (%)
USSP15	117±4	0.88
USSP30	111±3	0.96
USSP60	93±4	0.97
USSP120	21±3	0.98
USSP240	13±4	1.26
USSP360	12±3	1.38

A significant reduction in the crystallite size was observed, while the mean micro-strain was increased with the USSP duration. The crystallite size was reduced up to 12 nm in the USSP360 sample.

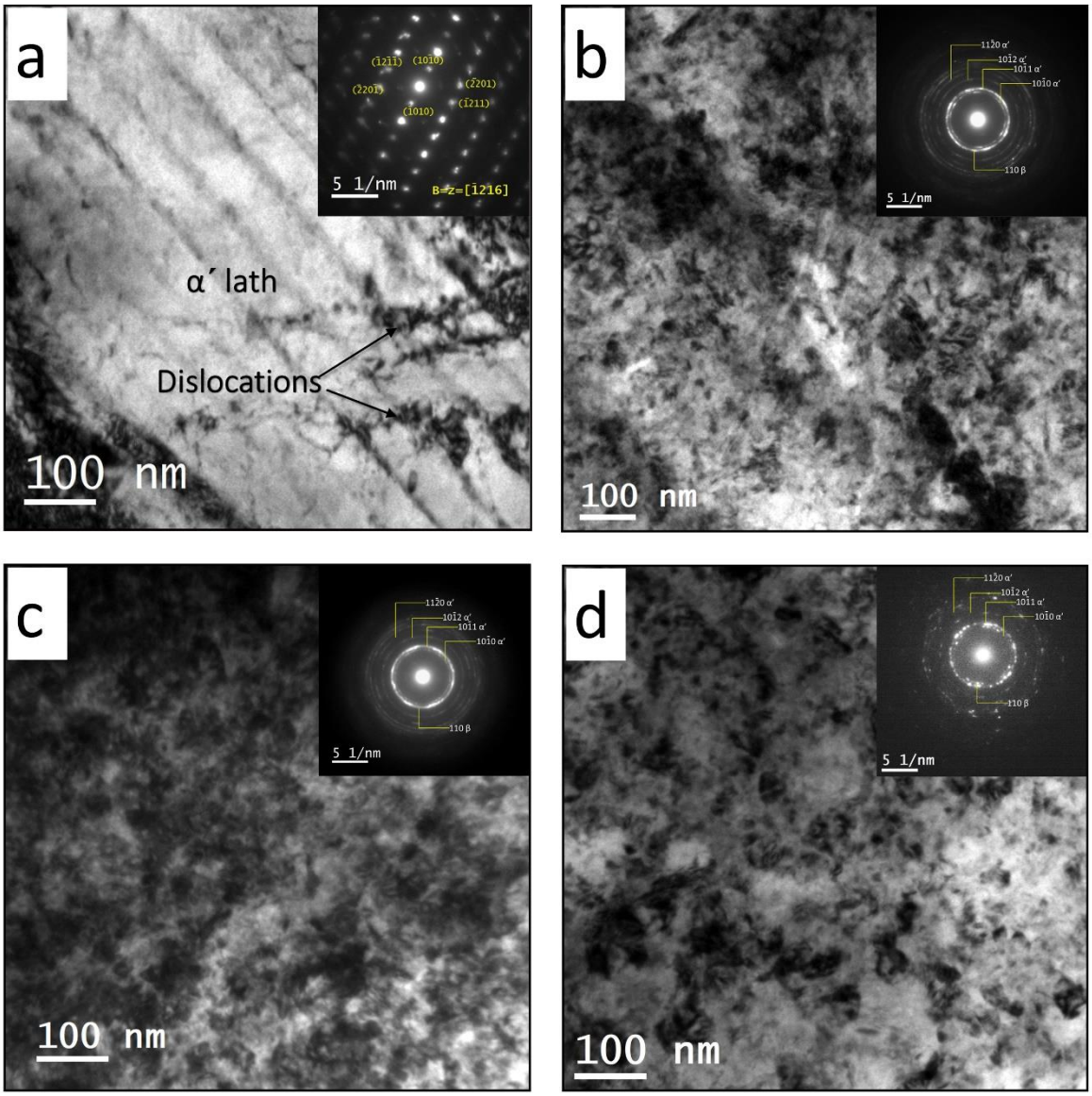

Figure 4.5 Typical TEM micrographs with respective SAED patterns, of the different conditions: (a) Un-USSP showing twins and dislocations, (b) USSP30, (c) USSP60, and (d) USSP120.

Figure 4.5(a-d) presents typical TEM micrographs of the Un-USSP, USSP30, USSP60 and USSP120 specimens, along with their corresponding selected area electron diffraction (SAED) patterns. In the Un-USSP specimen, α' platelets along with some twins and dislocations were observed (Figure 4.5a). After the USSP treatment, presence of the discontinuous ring-type patterns with discrete spots from the α′ and β phases in

the SAED images, indicates the formation of a large number of micro and nanograins in the USSP treated specimens (Figures 4.5b to 4.5d). Thus, large numbers of nanograins were formed in surface region of the USSP treated specimens. High densities of dislocations and dislocation tangles were also observed within the grains. All the USSP treated specimens showed reduction in the grain size. The variation in the contrast within the grains also suggests high internal stresses and lattice distortion [221].

4.3 SURFACE ROUGHNESS

Surface roughness of the different samples was measured using surface profilometer. The various surface roughness parameters for the Un-USSP and USSP treated samples are listed in Table 4.3 where, R_a, R_q, and R_z are the average roughness of the surface profile, root mean square roughness and average of maximum peak to valley for the five consecutive sampling lengths, respectively. For each sample, readings were taken at five different locations to calculate the average value. Variation in surface roughness (R_a) is presented in Figure 4.6. A significant increase in the surface roughness was observed in the USSP15 sample compared to the Un-USSP condition. However, there is gradual increment in the roughness with increase in the USSP duration from 30 to 360 s. Highest surface roughness was found in USSP360 sample. The SEM images of the Un-USSP, USSP30, USSP60 and USSP120 treated samples displayed in Figure 4.7 confirm the rough appearance of the USSP treated samples. Figure 4.7a of the Un-USSP sample shows much smoother surface than those of the USSP treated ones. Further, several micropores can be seen on the surface of the USSP30 sample (Figure 4.7b). Apart from micro-pores, some micro-cracks, cavities and surface inhomogeneities were also observed on the surface of the USSP treated samples (Figure 4.7(b-d)). Similar observations of pores and cracks were also reported for plastically deformed surface layer

of other materials [222–224]. The size and number of cracks were found to increase with the duration of the USSP treatment.

Table 4.3 Surface roughness* of the Un-USSP and USSP treated specimens.

Treatment Condition	R_a (µm)	R_q (µm)	R_z (µm)
Un-USSP	0.204±0.038	0.256±0.042	1.347±0.932
USSP15	1.127±0.128	1.156±0.163	6.693±0.643
USSP30	1.394 ±0.161	1.712±0.189	6.868±0.758
USSP60	1.593±0.103	1.915±0.127	6.484±0.612
USSP120	1.808±0.152	1.107±0.118	7.201±0.544
USSP240	2.004±0.184	2.391±0.163	8.345±0.634
USSP360	2.531 ±0.161	3.159±0.189	13.705±0.522

*R_a: Roughness average

*R_q: Root mean square (RMS) roughness

*R_z: Average maximum height of the profile

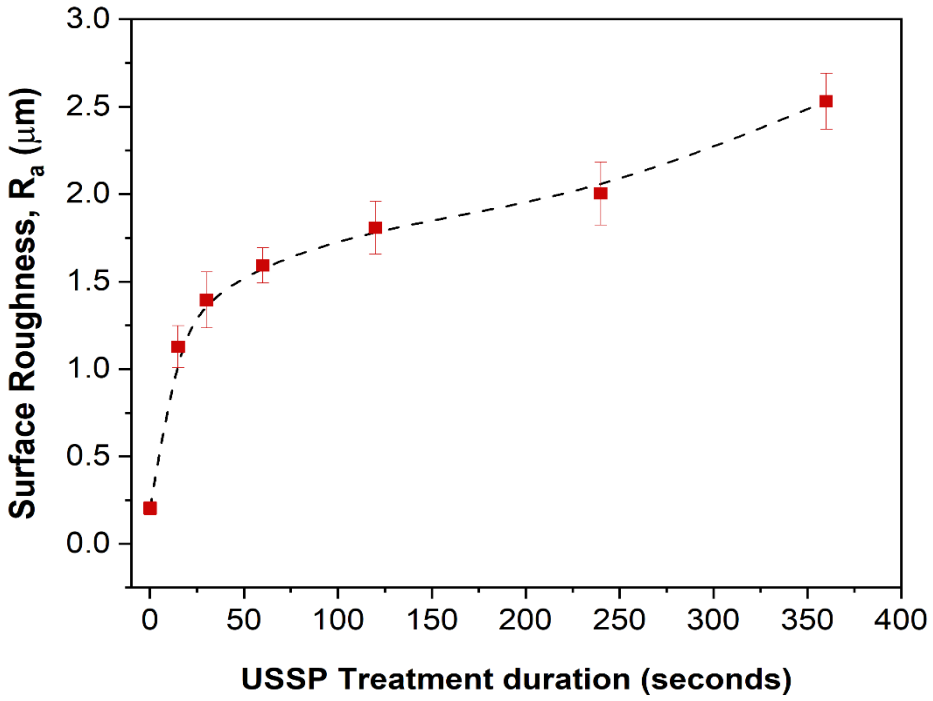

Figure 4.6 Variation of average surface roughness with duration of USSP.

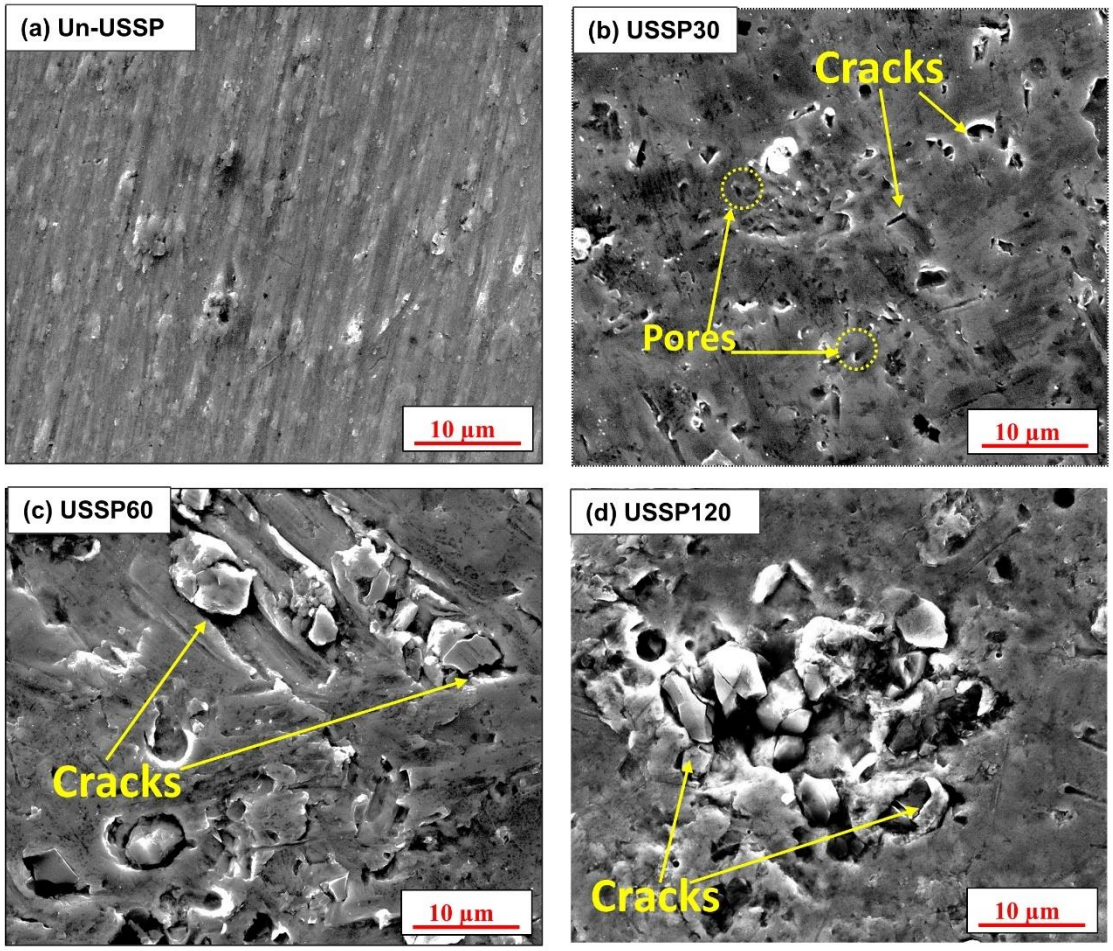

Figure 4.7 SEM images of the (a) Un-USSP, (b) USSP30, (c) USSP60 and (d) USSP120 specimen showing surface cracks.

4.4 MICROHARDNESS

Microhardness measurement was carried out on top surface of the Un-USSP sample and on the longitudinal sections (normal to surface) of the USSP treated samples. Microhardness was measured at three different locations and their average was taken. Figure 4.8 depicts microhardness profiles of all the USSP treated samples, from surface towards interior, which may be seen to be higher by 15-22%, close to the surface, and decrease gradually with depth. An improvement in microhardness was observed with increase in the USSP duration, and the depth of the affected region with appreciable increase in the hardness (~14-18%) can be seen up to 100 µm in Figure 4.9c.

Microhardness near the top surface and also the depth of the deformed layer increased with the duration of USSP treatment.

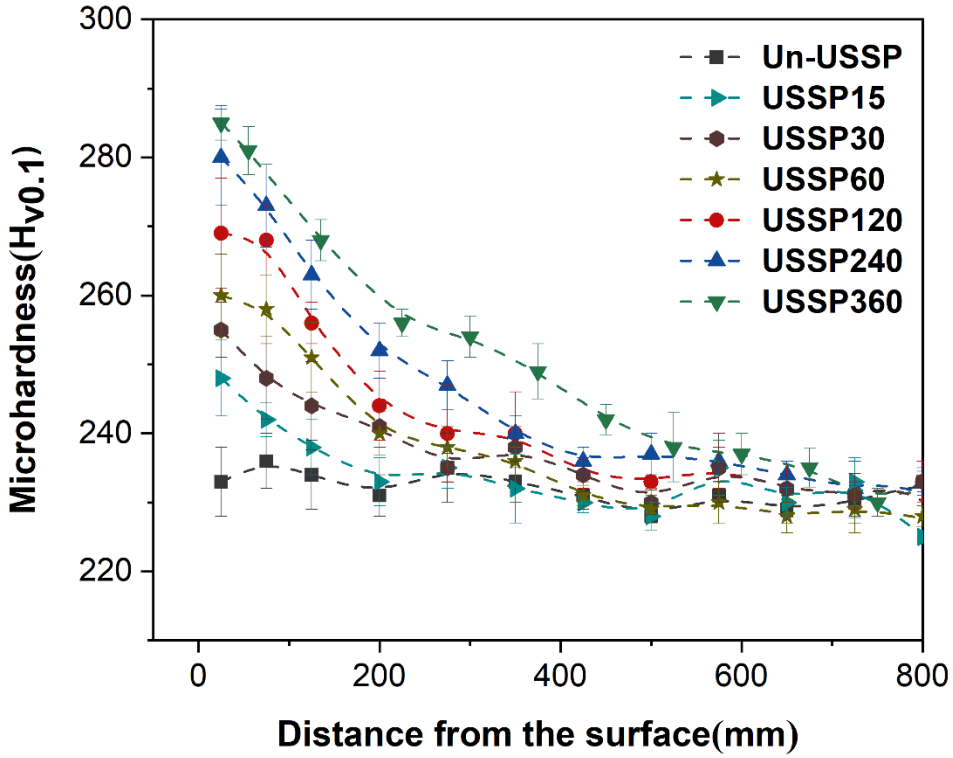

Figure 4.8 Microhardness variation along the depth of the Un-USSP and USSP treated samples.

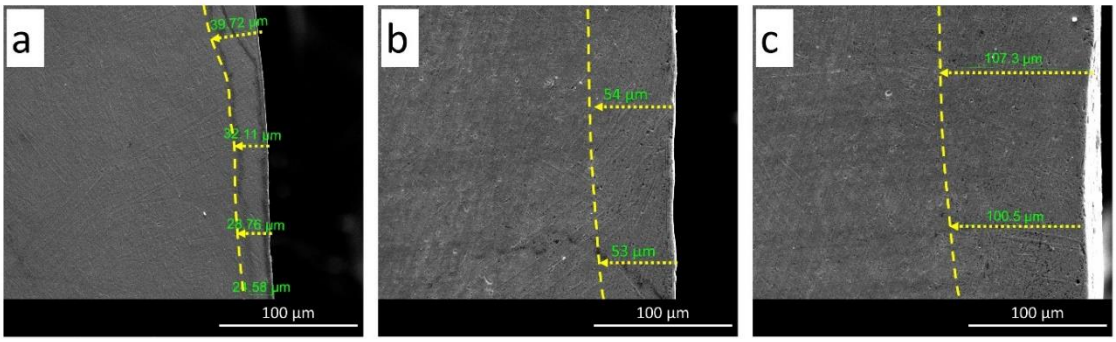

Figure 4.9 SEM micrographs of the (a) USSP120, (b) USSP240, and (c) USSP360 samples, showing depth of modified layer on the longitudinal mid-section of the specimens.

The typical SEM micrographs of longitudinal section (normal to surface) of the alloy Ti-13Nb-13Zr, USSP treated for 120, 240 and 360 seconds are shown in Figure 4.9. Surface modification resulting from USSP is shown by these SEM micrographs, up to the depths of ~35µm, ~54µm and ~103µm from the shotpeened surfaces of the samples USSP treated, for 120, 240, and 360 seconds, respectively.

4.5 RESIDUAL STRESS

The surface residual stress was determined for each specimen in the surface region using $\sin^2(\psi)$ method. The residual stress was determined at the top surface of the Un-USSP and USSP treated samples by measuring the inter-planar spacing of the $(10\bar{1}3)$ α' martensite plane, as a function of $\sin^2(\psi)$, ranging from 0 to 0.75 at interval of 0.15 (Figure 4.10). A step size of 0.07 degree per second and 2 seconds per step speed was used for the 2-theta scan from 79 to 86 degrees.

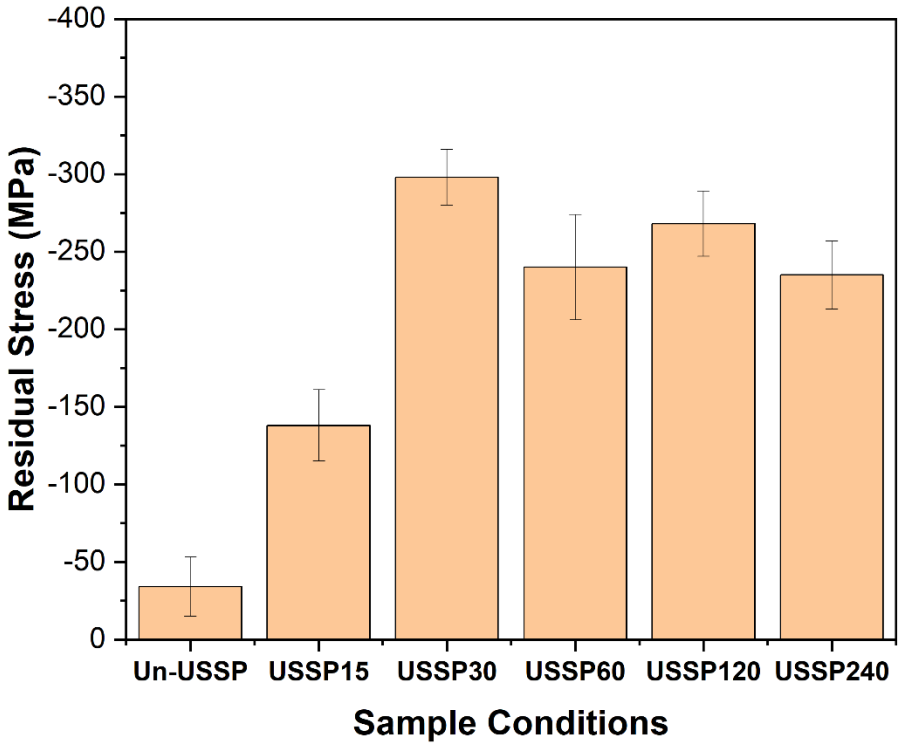

Figure 4.10 Surface residual stress of the Un-USSP and USSP treated specimens.

The maximum residual stress at the top surface of the Un-USSP sample was -53 MPa. The value of normal compressive stress was increased progressively with an increase in the USSP duration from 15 s to 30 s; however, there was relatively less increase from further increase in the USSP duration from 60 s to 240 s. The presence of compressive residual stress at the surface and subsurface region of the samples after the USSP treatment was also reported elsewhere [225].

4.6 DISCUSSION

4.6.1 Microstructure

Titanium alloys are known to transform into α′(hcp)/α′′(orthorhombic) martensite on water quenching from the β phase field, depending upon the composition of the alloy[212]. In the present investigation α′ martensite platelets formed from β phase of the Ti-13Nb-13Zr alloy on water quenching, following the beta phase solutionising at 900°C (β transus temperature ~735°C), in line with earlier observations [226].

The initial microstructure consists of acicular α' martensite in the β grain matrix as evident from the TEM micrographs and corresponding SAED patterns in Figure 4.2. Similar microstructure was also observed by Geetha et al. [70] in the β-solutionised and water quenched condition of the Ti-13Nb-13Zr alloy. After the USSP treatment, the lath type morphology of the Un-USSP sample (Figure 4.5a) was changed into small micro and nano-sized grains, as evident from the TEM micrographs of the different USSP treated samples, shown in Figures 4.5b to d. The discrete ring-type patterns in the SAED images suggest that the coarse grains were subdivided into small ones with wide orientation distribution. Formation of diffused ring-type pattern confirms the process of grain sub-division and formation of nanograins in the surface region. The occurrence of multiple diffraction circles with well-defined diffraction spots shows high angle

misorientations of microbands [227]. The elongation in diffraction spots indicates internal stresses [228]. The clustering of SAED patterns in certain rings suggests that several nano grained areas have common crystallographic orientation, implying that these nano grains evolved from larger grains.

With increase in the duration of USSP treatment, the discontinuous spotty diffraction (Figure 4.5a) was transformed into well-established continuous ring-type patterns (Figure 4.5b). It was due to repeated and multidirectional impacts of steel shots on the alloy surface, leading to increase in strains. It is obvious that at large strains, there is activation of different twin systems, and thus, twin-twin intersections took place. Lu et al. also reported multi-directional twin-twin intersections generated in 304 stainless steel, from multiple impacts of laser shock peening leading to refinement of grains at the top surface [229]. The large number of twins along with twin-twin intersections hinder the movement of dislocations generated, and therefore large number of dislocations accumulate at the twin boundaries. Deformation twins along with dislocation–twin boundary interactions, refine the microstructure into irregularly shaped nanograins with large misorientations, giving rise to a continuous ring-type pattern in the SAED pattern.

USSP is one of the severe plastic deformation processes that refines the microstructure, and the grains possess high strain energy and high dislocation densities [230]. In the high stacking fault energy materials such as aluminium and iron, dislocation glide dominates the process of grain subdivision, whereas in the case of low stacking fault energy materials such as copper, stainless steel, nickel-based alloy and titanium, the mode of deformation changes from dislocation slip to twinning with increase in strain [107]. As there are less easy slip systems in titanium alloys, twinning is initiated to accommodate initial strains and to reduce local stress inside the material, during plastic

deformation. At room temperature, with increase in strain rate, hcp materials begin to exhibit twinning as it is their preferred deformation mode [231]. In the earlier publications, deformation twins were observed in many titanium alloys [232,233]. According to Lu et al. grain subdivision mechanism in titanium consists of two steps: first the multi-directional twin-twin intersections at sub-micron level and second, the twin-dislocation intersections at nanometer level [234].

Mainly α´ and β phases were identified by XRD analysis in the Un-USSP and USSP treated conditions. However, no phase change was observed due to the USSP treatment, though there was decrease in volume fraction of the β phase with increase in the duration of ultrasonic shot peening, as indicated by the intensity of XRD peaks. The decrease in β phase can be associated with formation of strain-induced α´ martensite from the β phase matrix [235]. Broadening and shift in the XRD profiles of the USSP treated samples were observed, which is mainly due to grain refinement and mean micro strain [236]. The values of micro strain are consistent with one of the β-Ti alloy, with surface modified by SMAT technique [237]. The increase in the mean micro strain after USSP treatment can be due to distortion of lattice and elastoplastic surface changes caused by impingement of heavy steel shots [238]. Development of surface nanostructure was also proved from the reduction in crystallite size, as shown by the XRD (Table 4.2). The calculated values of crystallite size are in agreement with our previous findings [239].

4.6.2 Roughness and Microhardness

The USSP treated surface is more irregular than the untreated surface. It is therefore evident that the roughness increases with shot peening duration. High surface roughness in case of the USSP treated samples can be due to varied size peaks and valleys formed during initial impacts of shots, but with increase in the USSP duration,

subsequent impact of balls on these peaks and valleys causes flattening of surface irregularities. Initially, there was sharp increase in the roughness (USSP15); however, with further USSP treatment, it gradually increases up to 360 seconds of USSP treatment (USSP360). With increase in the USSP duration from 60 to 120 seconds, there is also an increase in the roughness and cracking tendency on the top surface of the samples (Figure 4.7). With further increase in the USSP duration to 360 seconds, there was deterioration of the surface and increase in the roughness. Surface cracking caused by USSP is dependent on the nature of material; for example, materials with low stacking fault energy, such as high nitrogen austenitic stainless steel, have shown cracks from USSP even for less than 10 minutes [240]. Due to excessive work hardening, materials with low stacking fault energy work harden quickly and break, especially at high strain rates.

In general, for high fatigue life, surface roughness should be as minimal as possible. The increase in roughness decreases the effective compressive residual stress on the material surface by creating stress concentration [241]. The increase in microhardness near the top surface in the USSP treated specimen can be ascribed to grain refinement and induced compressive residual stresses. There is gradual decrease in the microhardness, which can be attributed to gradient change in the microstructure from the USSP treated surface towards interior, consistent with the earlier observation [127]. During severe plastic deformation, the high strain rates generate dislocations which multiply and in turn increase work hardening of the material. Work hardening, together with grain refinement leads to an overall improvement in the hardness of the USSP treated samples.

4.6.3 Residual Stresses

Nanograins at the surface and gradient microstructure towards the interior have been the characteristics of the surface treated materials [242]. Several investigators have also reported high compressive residual stresses in the surface layer after the USSP treatment [107,243,244]. Kumar et al. [245] have shown increase in the surface compressive residual stresses with increase in the duration of SMAT. Surface compressive residual stresses are also introduced inside the material after the USSP treatment (Figure 4.10). Also, there is formation of gradient microstructure. The magnitude of associated compressive residual stress is highest at the surface and decreases with increase in depth from the shot peened surface. The residual stress is relieved in the cracked region. In the present investigation, the residual stresses are correlated with the microstructural changes occurring from the process of severe plastic deformation. Roland et al. [246] partially ascribed the near-surface residual stresses to high dislocation density inside the material.

4.7 CONCLUSIONS

Surface grain refinement of the alloy Ti-13Nb-13Zr was induced through USSP technique. The grain refinement occurs from the combined process of twin-twin and twin-dislocation interaction. Following conclusions are drawn from this chapter:

1. The process of USSP successfully developed nano size grains of ~21, ~13 and ~12 nm in the top surface of the alloy after 120, 240 and 360 seconds of USSP. TEM and XRD analyses confirmed the formation of nanostructure in top surface of the samples.
2. No phase transformation was observed in the alloy after USSP treatment.

3. Microhardness of the USSP treated specimen increases with increase in USSP treatment duration and the depth of deformation also increases with increase in USSP duration.
4. With increase in the USSP duration, there is also an increase in the roughness and cracking tendency on the top surface of the samples.
5. There is also an increase in compressive residual stress with increase in the USSP duration. However, residual stress is relieved from higher duration of USSP due to localized cracking.